Journal of Applied Electrochemistry **31**: 739–748, 2001.

Methanol-resistant cathodic oxygen reduction catalysts for methanol fuel cells[†]

H. TRIBUTSCH, M. BRON, M. HILGENDORFF, H. SCHULENBURG, I. DORBANDT, V. EYERT, P. BOGDANOFF and S. FIECHTER
Hahn-Meitner-Institut, Dept. Solare Energetik, 14109 Berlin, Germany

Received 18 January 2000; accepted in revised form 9 September 2000

Key words: biocatalysis, catalysis, methanol insensitivity, oxygen reduction, Ru–carbon–carbonyl complexes

Abstract

Efforts were made to simplify the structure of Ru-based catalysts, and to tailor industrially practicable methanol insensitive oxygen reduction catalysts both by thermolysis of Ru-carbonyls in organic solvents and by modified preparation techniques of Ru colloids. Selective catalysis was found to be essentially independent of the chalcogene (Se) used which, however, is a crucial factor for facilitating efficient electron transfer. All preparations contained Ru-metal particles of nm size, the surfaces of which were modified by carbonyl and carbido-carbonyl complexes or carbon compounds. The role of carbon as ligand to Ru clusters stabilizing the Ru interface against oxidation and in promoting catalytic electron exchange via nonbonding Ru d-states is theoretically analysed in a model calculation. An analogy is drawn to a biological Fe – only hydrogenase centre in order to discuss projected key experiments for optimizing reduction catalysis: the stabilization of small, inherently unstable catalytic metal clusters by CO or CN and their linking via electron bridges such as S and Se to electron reservoirs (metal colloids).

1. Introduction

The original aim of this research was the development of a reversible oxygen electrode, an electrode which, under illumination, is able to efficiently oxidize water to molecular oxygen and which is also able to reduce oxygen to water efficiently in the dark. Such a system would be useful for both photoelectrolysis of water and the reverse reaction, namely, the production of electricity via oxygen and hydrogen consumption in a fuel cell. The main challenge for such a system is the catalysis of multielectron transfer.

Two strategies were employed towards the development of suitable catalysts. The first was the search for semiconducting materials which provided transition metal d-states as energy bands. Electronic charge carriers reacting via such d-bands could engage in metal centred electron transfer, thus allowing an interfacial coordination chemistry. In other words, the interfacial transition metal centres, while becoming oxidized or reduced, change the ligand configuration and adsorb or release small ligand species. The success of this strategy was demonstrated with materials such as RuS_2, which, during illumination, oxidize water stepwise to molecular oxygen without corroding [1, 2]. The second strategy deals with the development of self-organized electron transfer mechanisms. The Markus theory of electron transfer is a theory based on the principle of reversibility. Consequently, this theory does not allow real (synergetic) multielectron transfer which would be the most energy efficient process for the oxygen electrode [3, 4]. Classical electron theory only permits stepwise subsequent electron transfer. This implies the generation of intermediates, the redox properties of which have to be optimized, to allow an efficient overall multielectron transfer process. However, far from thermodynamic equilibrium, electron transfer is also possible, allowing new mechanisms. For such reactions, autocatalysis is important. During electron transfer, some electronic and structural parameters must change in such a way as to facilitate subsequent electron transfer. If the respective feedback mechanisms are optimized, the first electron can slave the transfer of the subsequent ones and an overall multielectron transfer is feasible, as deduced from model calculations. Both, kinetic effectivity and energetic efficiency can be improved with such synergetic mechanisms. The implications and preliminary examples of such processes have been discussed [3, 4].

On the basis of these strategies for identification and selection of possible materials for a reversible oxygen electrode [5] Chevrel-type compounds [6] of the composition $Mo_{6-x}M_xX_8$ (X = S, Se, Te) were chosen. As Figure 1 shows, the distribution of electronic states reveals the existence of pronounced d-bands bordering a forbidden energy region of range 1.4–1.7 eV. [7]. The

[†] Paper presented at the workshop on "Electrocatalysis in direct and indirect methanol fuel cells" held at Portoroz, Slovenia, September 1999.

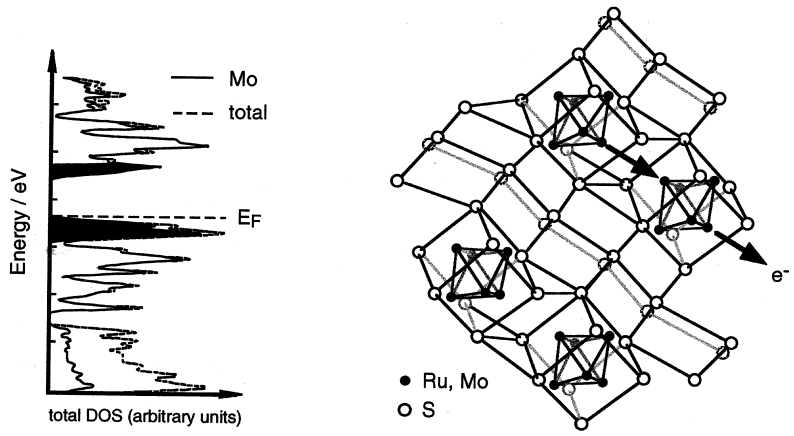

Fig. 1. Scheme of electronic states of $Ru_2Mo_4Se_8$ (left, simplified after [7]) and related Chevrel phases and of the crystal structure (right) indicating that electrons exchange occurs via d-bands bordering the energy gap (dark areas) and via the mixed metal octahedral clusters.

Fermi level varies with the nature of the metal included in the mixed cluster besides the molybdenum. The presence of Ru in the composition $Ru_2Mo_4Se_8$ places the Fermi level near the top of the valence band, making the compound a degenerate p-type material. As a consequence of the high density of d-states near the Fermi level in the range of the valence band, cathodic electron transfer directly exchanges electrons via the octahedral mixed metal clusters (Figure 1, right). Semiconducting transition metal compounds with d-character have shown characteristic activity with respect to redox systems. For FeS_2, which has iron d-bands as valence and conduction bands, for example, a very clear difference in electron exchange efficiency is shown between redox partners that can coordinate to the surface iron (such as I^-, Br^-, OH^-) and those which cannot (e.g., $Fe^{2+/3+}$, $Fe(phen)_3^{2+/3+}$, $Fe(bipy)_3^{2+/3+}$) [2]. The reason is that, after the photogenerated holes are trapped in the surface iron, the oxidation state of the iron is increased and electron-donating species coordinate as ligands, thus enabling efficient electron transfer. Species such as $Fe^{2+/3+}$ do not have the tendency to coordinate with oxidized interfacial iron. Correspondingly, the observed electron transfer efficiency and oxidative reactivity is low. Summarizing, d-band materials allow an interfacial coordination chemistry. This is a basis for selectivity since molecules that cannot coordinate will show a much smaller rate of electrochemical activity [8].

Additional interesting catalytic properties arise from the presence of octahedral mixed metal clusters. They act as reservoirs for electron transfer to the electrochemical species coordinated to the clusters and, in addition, the clusters can change volume. When, as a consequence of metal substitution, or during a four-electron transfer reaction, the cluster looses four electrons, it becomes weaker bonded and increases in volume by approx. 15%. Such a correlation between electron transfer and structural dynamics may function in the direction of a stimulated or cooperative electron transfer since autocatalysis (feedback) is involved [3, 4]. At present, however, knowledge about the structural dynamics of Chevrel phases does not allow a more detailed description of such a nonlinear electron transfer process which occurs far from equilibrium.

The Chevrel phase $Ru_2Mo_4Se_8$ became one of the best oxygen reduction catalysts in acid solution [5] besides platinum and more promising than macrocyclic complexes, especially those related to porphyrins and phtalocyanins [9], and transition metal oxides such as perovskites and pyrochlore structured oxides [10]. Additional favourable properties of the Chevrel phases were long-term stability and selectivity. However, they have a significant drawback in being difficult to synthesize. They are characterized by a very narrow formation range in the region of 1500 °C and the output of growth procedures aimed at crystal preparation is modest. There was, therefore, a definite need to simplify the preparation technique.

In an effort to synthesize Chevrel compounds at low temperatures carbonyl complexes of the metals were added to a heated xylene solution together with a respective chalcogene. Nanocrystalline-amorphous compounds of the composition $Ru_xMo_ySe_yO_z$ were obtained with preparation procedures requiring temperatures of only about 150 °C. The favourable properties of these catalysts, as well as the simple preparation technique, motivated further studies.

2. Experimental details

2.1. *Catalyst preparation*

2.1.1. *Preparation by thermal reaction (preparation A)*

Powder of the catalyst was prepared by thermolysis and reaction of a ruthenium-precursor, usually $Ru_3(CO)_{12}$, in an organic solvent varying the selenium, and ruthenium carbonyl content. A fixed amount of selenium was dissolved in 200 ml of the hot organic solvent (xylene), which had been deaerated with argon for 30 min. 145.6 mg of $Ru_3(CO)_{12}$ was added to the solution,

which was refluxed for 20 h. The amount of added selenium was varied from 0 (selenium free catalyst) to 9 mg (see results for details). The highest amount of selenium was 14.3 mol %, related to the total amount of ruthenium and selenium. In another series of experiments, the time of thermolysis was varied between 0.5 and 78 h, whereas the selenium concentration was kept constant (saturated solution). The catalysts were typically prepared in xylene, but other organic solvents such as nonane and tetradecane were also tested. After the reaction was finished, the black solution was filtered. A black residue and a colourless or red filtrate, depending on the initial selenium concentration, were obtained. The black powder was dried at 90 °C in air overnight, yielding 50 to 90 mg of catalyst, depending on the selenium content and the time of synthesis. Carbon supported catalysts were obtained via the same procedure but with addition of carbon to the reaction solution.

2.1.2. *Catalyst synthesis via preadsorbed $Ru_3(CO)_{12}$ (preparation B)*

A carbon supported catalyst containing about 20% ruthenium was prepared by thermal decomposition of $Ru_3(CO)_{12}$. The details of the method applied will be described in a subsequent publication. Briefly, $Ru_3(CO)_{12}$ was supported onto carbon base from an organic solvent under mild conditions and thermalized after solvent removal under inert or hydrogen atmosphere. The incorporation of selenium was also possible.

2.1.3. *Catalyst synthesis via colloidal Ru-nanoparticle (preparation C)*

To prepare a catalyst via colloidal Ru nanoparticles we followed a procedure described by Bönnemann et al. [18]. A tetrahydrofurane (THF) soluble ruthenium colloid powder was obtained by reduction of a solution of 2.8 g $RuCl_3$ in 500 ml THF with 100 ml of a 0.4 M solution of $N(C_8H_{17})_4BEt_3H$ in THF. After addition of 100 ml absolute ethanol the solution was centrifuged (4500 rpm, 15 min) and the solid washed twice with ethanol and dried under argon. The powder obtained was very soluble in THF and had a metallic ruthenium content of of 67%.

Support of the nanoparticles ($d \simeq 1$ nm) onto carbon was performed by adsorption of the colloids in organic solvent. A final catalyst typically contained up to 23% Ru with an estimated (XRD) Ru particle diameter of 3 nm and 77% carbon and, optionally, also small amounts of Se (~1%).

2.2. *Electrode preparation for electrochemical experiments*

The electrocatalytic activity of the powder materials was tested using rotating disc electrode (RDE) measurements. The electrodes for RDE experiments were prepared following a method proposed by Schmidt et al. [19]. 1 mg of the catalyst powder was suspended in 0.5 ml deionized water and sonicated for at least 30 min. 5 μl of this suspension was pipetted onto a glassy carbon rod of 3 mm in diameter and dried in air and afterwards at 90 °C for 10 min. The catalyst layer was then covered with a thin Nafion® layer by adding 2.5 μl of diluted Nafion®-solution (0.1875% in EtOH), drying in air at 90 °C. Catalyst loadings of 142 μg cm^{-2} were obtained for unsupported catalysts. This catalyst loading, which was higher than that proposed by Schmidt et al., was used to obtain diffusion limited currents in the RDE-measurement even at higher rotation speed as well as to achieve loadings typical of fuel cell applications.

For the electrochemical characterization of the carbon supported catalyst 10 mg of catalyst were suspended in 2 ml ethanol containing 0.09% Nafion®. This suspension was ultrasonicated for at least 20 min and 5 μl were subsequently pipetted onto a glassy carbon electrode and dried for 5 min in air. The loading with Ru of a carbon supported electrode prepared in this way was estimated to be 70 μg cm^{-2} (preparation B and C).

2.3. *Analytical techniques*

2.3.1. *Thermogravimetry*

The thermal stability of the prepared Ru-catalysts was investigated using a Netzsch STA 409C thermobalance. Typical heating rates of the furnace, where the sample was decomposed and where the heat of decomposition was simultaneously monitored against a reference sample, ranged from 5 to 10 °C min^{-1}, respectively. The amount of sample used for the experiments was about 25 mg. The temperature and time dependent decomposition was studied under a continuous nitrogen gas flow of 100 ml min^{-1}. Before and after the heat treatment the crystallinity of the sample was checked by X-ray diffractometry.

2.3.2. *X-ray diffractometry*

>The catalysts prepared were crystallographically analysed employing a Siemens X-ray diffractometer (D500/5000) with CuK_α radiation and $\Theta - 2\Theta$ coupling. Due to the small particle size exposure times up to 24 h were chosen.

2.3.3. *Mass spectrometry*

To analyse the gas species released at elevated temperatures catalyst powder was placed at the end of a closed quartz tube which was connected at the open end with a vacuum system pumped by a turbo pump. The tube was heated continuously by a programmable temperature controller up to 1000 °C using a heating rate of 100 °C h^{-1}. A Balzer's quadrupole mass spectrometer (QMS 420) was used in cross beam configuration to analyse the released gas species.

3. Results

3.1. *Properties of the $Mo_xRu_ySeO_z$ catalyst*

The $Mo_xRu_ySeO_z$ compounds actually showed a behaviour comparable to that of Ru-based Chevrel phases [11].

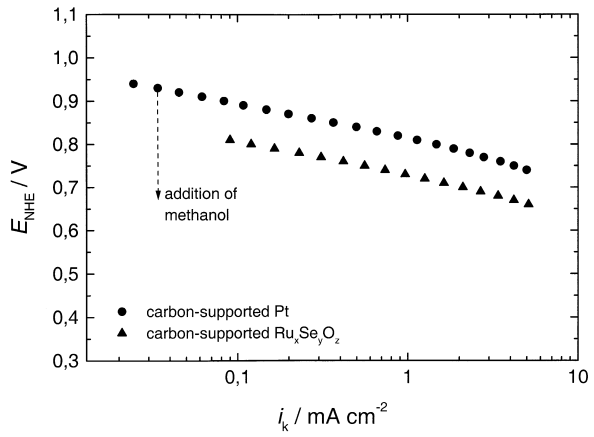

Fig. 2. Current–voltage characteristic (Tafel plots) of the $Ru_xSe_yO_z$ catalyst (preparation A) and of Pt in absence and presence of 1 mol l^{-1} methanol (in the case of Pt only an arrow is shown to indicate the effect of depolarization).

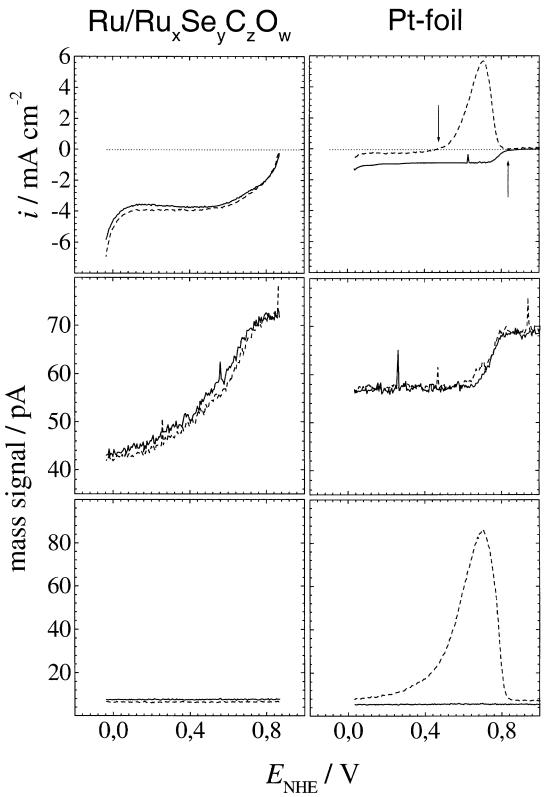

Fig. 3. Current voltage characteristics and parallel differential mass spectroscopic data (DEMS) on oxygen and CO_2 turn over at a $Ru_xSe_yO_z$ catalyst (preparation A) and on a platinum foil (arrows indicate range of methanol oxidation).

It turned out that molybdenum was not needed for catalysis. The stoichiometry of the catalyst therefore should read $Ru_xSe_yO_z$. However, since much carbon is contained (see below), the hypothetical new composition should be $Ru_xSe_yC_wO_z$. Figure 2 shows a current–voltage diagram comparing the behaviour of the catalyst with the behaviour of platinum. The laboratory electrodes of composition $Ru_xSe_yC_wO_z$ showed a similar favourable oxygen reduction potential but smaller current densities. However, although platinum significantly depolarized after addition of one mole methanol per litre, no change was observed in the current–voltage characteristic of ruthenium based nanocrystalline catalyst or d-band ruthenium compounds [12]. Figure 3 compares the electrochemical behavior and the differential electrochemical mass spectroscopical (DEMS) data for both, the $Ru_xSe_yC_wO_z$ compound and of a platinum foil. It is seen that platinum shows a clear oxidation current at potentials between 0.4 and 0.8 V vs NHE due to methanol oxidation while there is no such current with Ru-based catalyst. In the same potential region, platinum shows liberation of carbon dioxide due to the oxidation of methanol but there is no sign of carbon dioxide liberation in the case of Ru-based catalyst.

Although electrochemical and DEMS results were very similar for Ru-based Chevrel phases and nanocrystalline-amorphous Ru-phases containing the same elements there were no additional experimental data supporting the conclusion that the nanocrystalline compound also has a Chevrel type structure. The interesting properties of the Ru-based catalyst prepared from carbonyls in organic solvents attracted the interest of other groups, especially that of Hamnett [13, 14], Behm [15], and Alonso-Vante [16]. Although Hamnett et al. found compounds of composition MRu_5S_5 on carbon black (with M = Rh or Re) most active, Alonso-Vante concluded, on the basis of EXAFS-measurements [17], that the catalytic compound obtained has the composition Ru_xSe_y [16]. Gasteiger et al., on the other hand, came to the conclusion that the catalytic activity of the solution grown Ru-compound is basically the activity of pure Ru-metal [15]. Our group in turn followed a different approach towards the characterization of the catalytical active center which will be described hereafter.

3.2. *What is the catalytic centre of $Ru_xSe_yC_wO_z$?*

Transmission electron micrographs of the $Ru_xSe_yC_wO_z$ catalyst grown by methods A,B,C show basically metallic Ru nanoparticles of diameter about 4 nm which appear to be separated by an amorphous layer at the particle surface (Figure 4). This impression is supported by XRD patterns of the catalysts as grown and after anealing under argon at 240 °C (Figure 5). Broad diffraction lines are visible which can be assigned to the X-ray pattern of Ru-metal in colloidal form. Independently of the TEM-measurements a value of 4 nm particle size was inferred from FWHM analysis of the peaks using Scherrer's equation. When the catalyst is heated up to 240 °C a weak shoulder is observed at $2\Theta = 33°$. It can be interpreted as a Ru–Ru distance of Ru in an amorphous state. It was concluded that, on the surface of metallic Ru-colloids of 4 nm, an amorphous film of Ru-compounds is present which arises from decomposition of Ru complexes at elevated temperature. Both, the microscopic particles and the X-ray diffraction patterns did not change significantly with

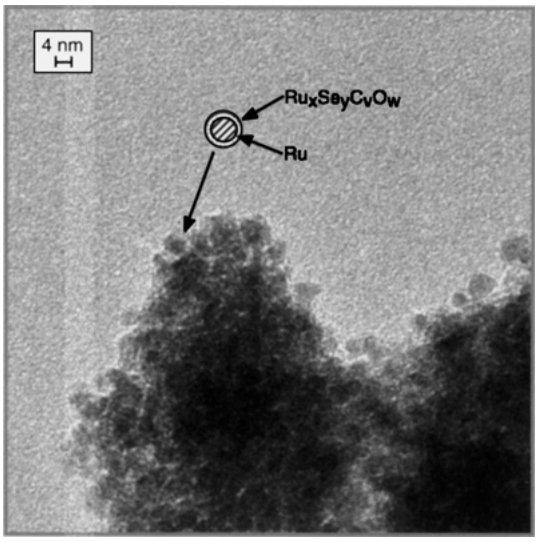

Fig. 4. TEM picture of a $Ru/Ru_xSe_yC_vO_w$-catalyst. Metallic nanoparticles (preparation A) of ruthenium (~4 nm dia.) are apparently covered by an amorphous layer containing Ru compounds.

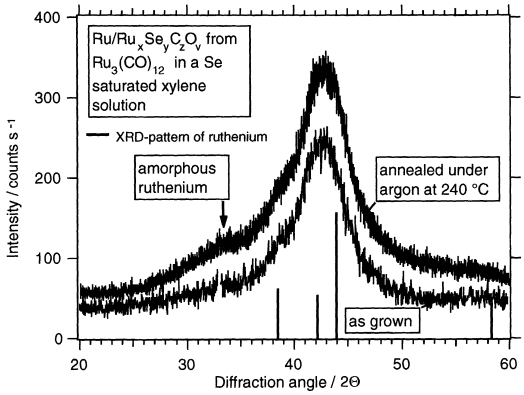

Fig. 5. XRD-patterns of a $Ru/Ru_xSe_yC_vO_w$-catalyst as grown and after annealing under argon atmosphere at 240 °C.

addition of Se during synthesis. Specifically, no crystallized Ru_xSe_y phase was found.

To test the influence of carbon species (i.e., carbonyls) on the catalyst composition and function three experimental strategies were adopted. The first consisted in looking for different synthesis routes. As described in the experimental part (preparation B and C), carbon supported catalysts were prepared via colloidal Ru precursors in organic solvent and via thermal decomposition of $Ru_3(CO)_{12}$. A comparison of Figure 6 and Figure 2 shows that a comparable catalytic efficiency for oxygen reduction is obtained.

In both preparation techniques (B and C) selenium was observed to improve the current density, but did not affect the overpotential for catalysis at 0.1 mA cm^{-2}. The second experimental approach involved thermogravimetric experiments including mass spectrometry for characterization of different catalyst preparations (Figure 7). When the active catalyst produced by thermolysis was heated above 90 °C and the released gas species were measured, the ionized products CO^+

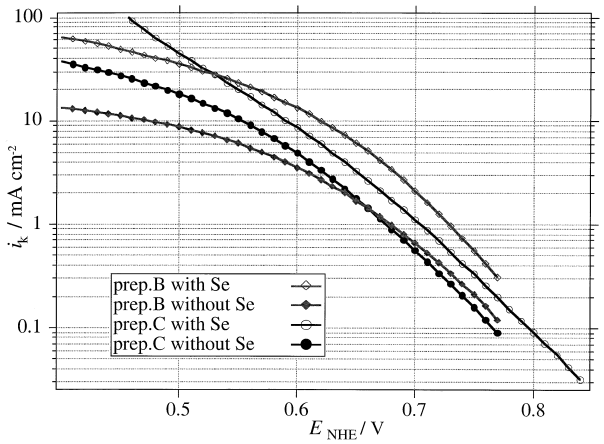

Fig. 6. Comparison of Tafel-plots of Se-containing catalyst with corresponding plots of Se-free catalysts grown by both, thermal decomposition (preparation B) and colloid preparation. Se is improving the current density, but not affecting the overpotential.

and CO_2^+ with a specific mass of 28 and 44, respectively, were the main products. The abundant presence of CO_2 is additionally indicated by the presence of the ionized fragments CO^+ (mass 28), C^+ (mass 12) and O^+ (mass 16). Most remarkable was that the colloidal catalysts, prepared by methods B and C, when investigated by thermogravimetry coupled with mass spectroscopy, also released significant amounts of organic species including CO and CO_2. From this observation it must be concluded, that the Ru-surface, in the case of Ru-colloids, is also modified by carbon species. Such experiments were extended to a commercial Ru catalyst (Ru/Vulcan (E-Tek)) which showed comparable activity in oxygen reduction catalysis. Release of abundant CO and CO_2 was also observed. The presence of stabilizing carbon containing ligands may, in fact, be the reason why the small Ru-particles do not immediately oxidize and ignite due to RuO_2 formation. Because of the release of carbon species from the catalyst at elevated temperature, the catalyst composition changes. These changes can be observed via the thermogravimetric curves [20]. They indicate that the catalyst grown by thermolysis looses carbon species in well defined steps. While the Ru carbonyl $Ru_3(CO)_{12}$ looses its CO between 150 and 250 °C, the Ru catalyst produced by thermal reaction looses CO and CO_2 between 250 and 350 °C and, in a second step above 600 °C. This indicates that specific interaction compounds are formed, which differ from carbonyl bonding in $Ru_3(CO)_{12}$ and which show a stronger carbonyl bond to Ru. When carbon species are released from the catalyst at elevated temperature (preparation A) the catalyst significantly looses catalytic activity [20]. For the other preparations (B,C) and for a commercial product (Ru/Vulcan (E-Tek)), the thermogravimetric curves yielded less conspicuous steps, but also showed a loss of carbon species with increasing temperature.

The third experimental strategy investigated the nature of carbon species formed during thermolysis. It was found that the best catalytic property was obtained

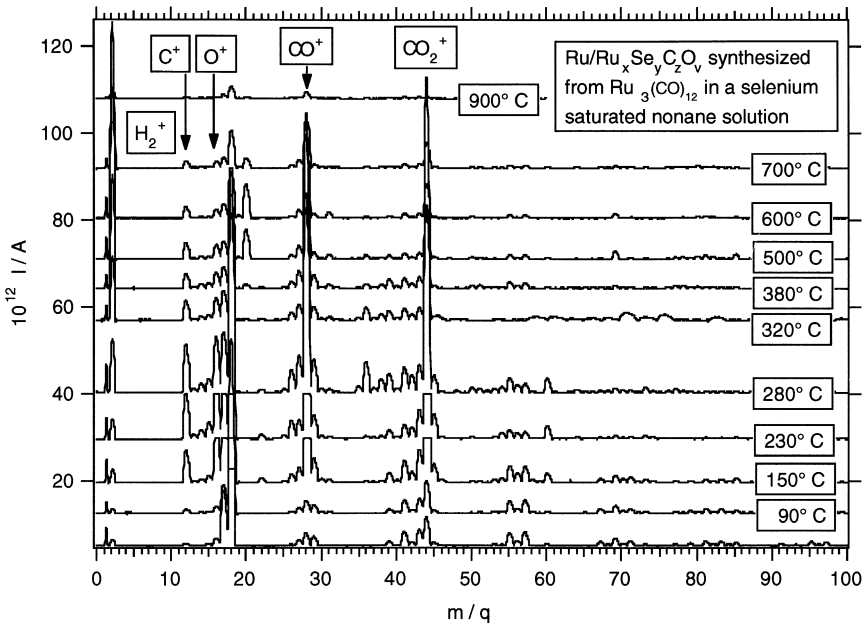

Fig. 7. Mass spectra of gas species released from a $Ru/Ru_xSe_yC_zO_v$-catalyst (preparation A) as a function of temperature, the masses of CO_2^+, CO^+, O^+ and C^+ are indicated.

after a 3 h thermolysis, although only with a small product yield. During this period the appropriate catalytic centre is apparently formed. However, the yield of active catalyst powder increases up to a reaction time of about 20 h. A still longer reaction time leads to a decrease in catalytic activity. From earlier studies on metal organic Ru-compounds [21–23] it is well known that the reaction products of Ru-carbonyl in organic solvents are Ru-metal and Ru-carbido-carbonyl clusters. These are octahedral clusters of Ru which contain carbon in the centre and carbonyl groups outside. After three hours of refluxing $Ru_3(CO)_{12}$ in nonane as organic solvent, the compound $Ru_6C(CO)_{17}$ with 18.7% efficiency is obtained [21]. Xylene as organic solvent leads, after 3.5 h refluxing, to the formation of $Ru_6C(CO)_{17}$ and $Ru_6C(CO)_{14}(C_6H_4Me_2)$ with 6.9% and 16.4% efficiency, respectively. These complexes were also found in our experiments using infrared spectroscopy. It was observed that the amount of complex formed depends on the selenium concentration in the preparation solution. The higher the selenium concentration the lower the amount of complex [24].

Electrochemical studies of the Ru-carbido complexes showed very low catalytical activity for oxygen reduction. Since continued thermolysis should lead to ongoing decarboxylation it may be that a modified Ru-carbido-carbonyl complex is active in oxygen reduction catalysis. Since, in the presence of Se, less ruthenium carbido carbonyl complexes are found in the catalyst preparation solution; it may be concluded that selenium is facilitating the attachment of such complexes to the Ru-interface and also aiding in reducing the number of attached carbonyl groups. When the solution used for thermolysis of carbonyls during catalyst preparation was allowed to rest for a longer period at 200 °C and xylene equilibrium pressure, Ostwald-ripening of microcrystals occurred and a cubane-type compound of composition $(Ru)_4(CO)_{12}(\mu_3\text{-}Se)_4$ was formed with carbonyl groups attached to the cubane-type Ru_4Se_4 core [25]. This observation may indicate that such cubane-type clusters are also present at the surface of Ru-colloids and have served us to perform model calculations to understand their properties (see below).

It was found that selenium is an important component for improving the current density generated by the catalyst, but its omission neither affected the low overpotential of the catalyst nor the methanol insensitivity (Figure 8). However, it is obviously involved in electron transfer to the catalytic center. Its role may be analogous to that played by sulfur in related catalysts [10] and to the role of sulfur in Vulcan-carbon when it

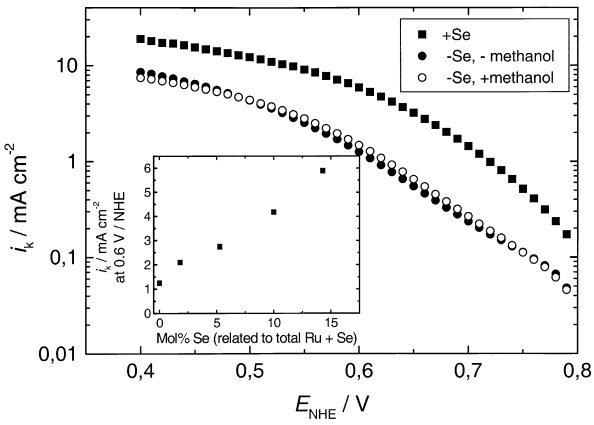

Fig. 8. Comparison of Tafel plot of $Ru/Ru_xSe_yC_vO_w$ catalyst with the performance of Se free $Ru_xC_vO_w$ catalyst in presence and absence of 1 mol l^{-1} methanol. In all cases synthesis occurred by thermal reaction.

improves catalysis of attached catalyst particles. However, it cannot be excluded, that selenium is present in the reaction centre affecting the rate, but not the overpotential, when structural dynamics is involved in catalysis. The presence of selenium may facilitate adiabatic electron transfer dynamics, while the absence of selenium (CO replacing Se) may involve nonadiabatic effects, so that the adiabatic rate transmission factor, κ_{ad}, has to be multiplied by a factor $P = 1 - \exp(-z\Delta^2)$, with z depending on nuclear dynamics and Δ representing the splitting of energy surfaces: $\kappa_{ad} \rightarrow P\kappa_{ad}$ (e.g., [26]).

4. Discussion and theory

4.1. *A ruthenium interface modified by carbon species as model catalyst*

The conclusion that our catalyst is not identical with a metallic Ru surface is supported by its high catalytic activity for oxygen reduction, the low (4%) rate of H_2O_2 production, its inability to spontaneously oxidize, as well as by thermogravimetric and XPS data [27]. Since all catalysts are loaded with organic matter and carbonyl or carbonylic groups we assume that the high catalytical activity of our catalysts is due to an interaction of nanocrystalline ruthenium and carbon ligands. The effect can be twofold: carbon species may stabilize the Ru metal interface, thus suppressing oxidation, which otherwise would transform Ru particles rapidly into RuO_2 particles in an exothermic reaction. The second effect of carbon species may be that of altering the distribution of interfacial electronic states by permitting Ru-complexes. This may explain why oxygen reduction is not preferring the H_2O_2 path, as in the case of pure ruthenium [28] and why higher catalytic activity and stability is achieved. For simplicity reasons, and because it may be sufficient to characterize the basic mechanisms involved, we will restrict our discussion on the expected promoting effect of CO groups only.

Neither pure ruthenium [28, 29] nor heated unsupported Ru based catalysts (preparation A), after release of carbon monoxide and carbon dioxide, are reasonable catalysts for oxygen reduction. But complexes between ruthenium and carbon or carbon monoxide are active. Some commercial nanocrystalline Ru samples, which show reasonable oxygen reduction catalysis (e.g., Ru/Vulcan (E-TeK)), are carbon supported and therefore contain carbon species. Ruthenium/carbido/carbonyl compounds are therefore expected to be the real catalysts. These complexes do not form a crystalline compound, but they are present as a film on the ruthenium colloids. A schematic drawing of such a bistructural catalyst is shown in Figure 9, which depicts the catalytic centres comprising ruthenium clusters with attached carbonyl ligands and to a smaller degree additional electron extracting complexes (CN, amino groups). Not all chemical bonds are saturated, but some bonds are unsaturated (dangling) so that an interaction

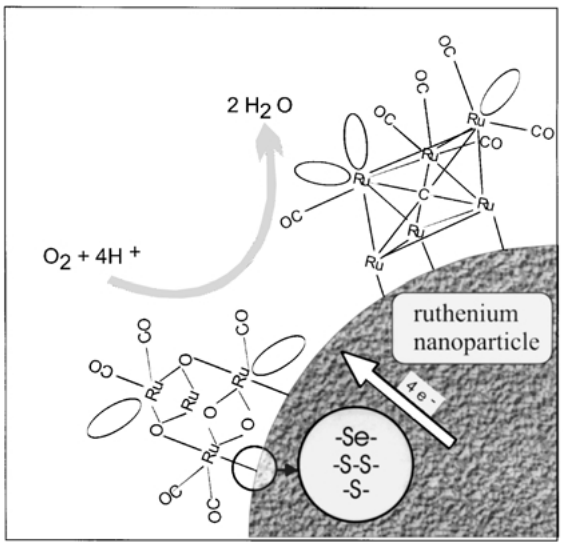

Fig. 9. Proposed qualitative structure of carbon modified Ru-catalyst. Possible interfacial Ru-clusters are shown grown on a Ru-nanoparticle. The cubane-like Ru-complex has been selected as a model system to describe the interaction of chalcogene with Ru-clusters during oxygen reduction. Selenium or sulfur may act as bridges to transfer electrons between the Ru-complexes and the colloids.

with oxygen can take place. Depending on the number of ruthenium in the cluster and the amount of carbonyl and other ligands, the chemical nature of these complexes will slightly vary, but in all cases they will accept electrons for oxygen reduction from the ruthenium colloids which serve as electron transfer mediators.

Theoretical investigations of ruthenium complexes show an efficient splitting of ruthenium d-states near the valence band maximum. We performed band structure calculations as based on density functional theory, which used the augmented spherical wave (ASW) method [30]. As a model system the ruthenium chalcogen cubane [$(Ru)_4(CO)_{12}(\mu_3\text{-Ch})_4$; Ch = O, S, Se] was selected. It was synthesized from the catalyst solution (preparation A) in crystallized form so that crystal parameters could be determined reliably [25]. It is in a simplified form shown in Figure 9 on the surface of a Ru particle. Theoretically we expect similar results if oxygen is substituted for selenium.

The calculated distribution of electronic states is displayed in Figure 10. Here the orbital projected partial densities of states (DOS), corresponding to some orbitals, are included, since all other states play only a negligible role in the energy interval shown; energies are referred to the valence band maximum E_V. According to these results the electronic structure is influenced by the strong CO bonding, which leads to a large splitting into bonding and antibonding states (at ± 5 eV) as well as by the metal ligand bonding. The latter gives rise to a manifold of very sharp Ru d-bands of t_{2g} like symmetry just below E_V, which have small admixtures from the chalcogen 4p states due to p-type overlap. While these states are bonding below 1.3 eV from the top of the

valence band ($E - E_V$) = 0, states near the valence band maximum are antibonding.

When few carbonyl ligands are present, there are many electrons in the cluster and most nonbonding orbitals are occupied. Consequently the ruthenium complex has moderate stability. In contrast, when there are many carbonyl ligands, many electrons will be extracted and as the consequence the antibonding orbitals are not occupied and the bonding orbitals generate a high stability (CN-groups or amines can replace carbonyl as electron acceptors). The best catalytic activity is apparently at an optimum between these two extreme cases. It is seen from the distribution of electronic states that the states which can be attributed to a ruthenium oxygen bonding during oxygen reduction catalysis are placed in the vicinity of the Fermi level. That means that electron transfer to oxygen chemisorbed to the ruthenium complex will be highly probable since we are dealing with isoenergetic electron transfer processes. Selenium, which has been used as a component in ruthenium catalysts for oxygen reduction, as discussed before, may play the role of electron transfer promotor, since its states, when interacting with ruthenium, are in the same energetic region as those responsible for the oxygen bonding to ruthenium. Since selenium is a better ligand than oxygen for electron transfer, it may act as electron transfer promotor between the ruthenium complex and the ruthenium colloids. The same can be assumed for sulfur which also can function as bridge (–S– or –S–S–) mediating electron exchange between the catalytic center and the colloids. This assumption might also explain why S-containing carbon bases or substrates (e.g., Vulcan) improve catalytical activity. However, even though the overpotential at 0.1 mA cm^{-2} is practically unaffected by addition of selenium ($\Delta E_{over} = 20$ mV), selenium may still be involved in the reaction centre. According to the calculated distribution of state density in the model cubane ruthenium–selenium–carbonyl cluster (Figure 10), selenium is responsible for antibonding states below the Fermi level. The more selenium present, the weaker bonded will be the ruthenium cluster. Its volume will correspondingly increase with the selenium content.

Summarizing, the catalytic activity can be understood in terms of a binary structure as presented in Figure 9, being composed of an electron reservoir (the Ru colloid) and the catalytic cluster centre (the Ru-cluster complex). The ruthenium clusters attached to ruthenium colloids are mostly stabilized by carbonyl ligands, which can be substituted by CN or amino groups. In contrast to pure Ru surfaces on which CO is readily oxidized in the potential region of oxygen reduction (0.4–0.8 V vs NHE), Ru complexes form stable compounds with CO, so that the bonds between CO and Ru are not fractured during electron transfer. Equally, a competing and destructive parallel chemical oxidation reaction is suppressed. Electrons are supplied to the ruthenium cluster for oxygen reduction via the ruthenium colloids. Oxygen and the intermediates which are formed during

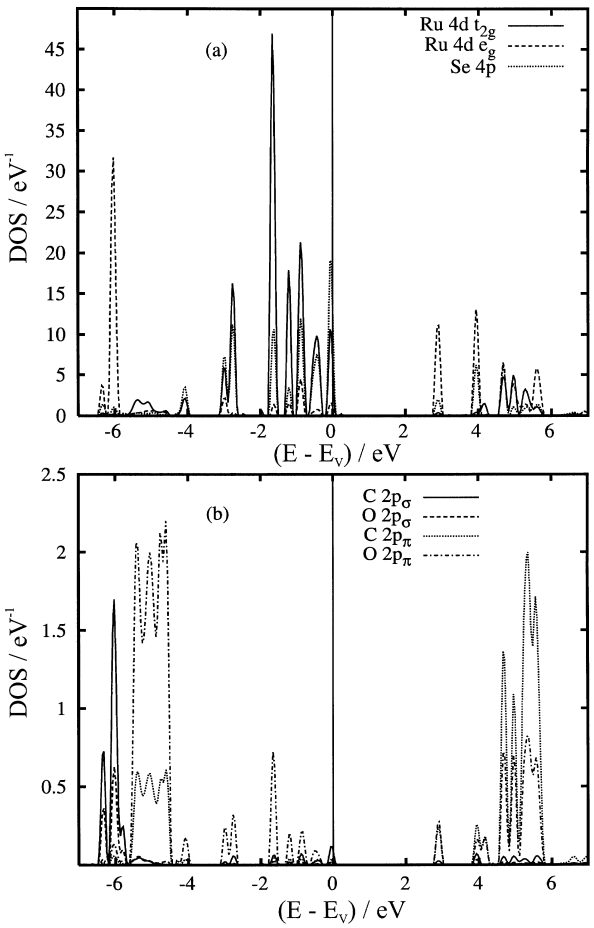

Fig. 10. Calculated densities of states in a cubane-type $Ru_4(CO)_{12}(\mu_3\text{-}Se)_4$ complex as synthesized from catalyst solution and indicated in Figure 9. (Se can be substituted for S and O without essential changes of the electronic structure). The high density of nonbonding (and catalytically active) Ru d-states near the Fermi level ($E - E_V$) (a) and the strong bond splitting (± 5 eV) produced by CO interaction (b) are indicated.

reduction to water are thereby coordinatively bound via the unsaturated bonds of the ruthenium clusters and electron transfer occurs near the Fermi level via nonbonding d-states. During this process the structure of the ruthenium cluster changes due to the change in the occupation of antibonding orbitals, which may add a non-linear component to multi-electron transfer [3, 4]. Selenium participates in such a cluster similar as oxygen and may thus have an effect on reaction dynamics. Interestingly the energetics of the catalytic reaction (the overpotential) is not affected by supplying selenium.

4.2. *Discussion of oxygen reduction electrocatalysis*

Many questions still remain open, including that of the detailed effect of selenium, yet the impression has gradually developed that the model (Figure 9) includes some basic features which deserve discussion. The recently resolved structure of the Fe-only hydrogenase of the bacterium Clostridium pasteurianum [31] is of interest. This is shown in a simplified way in Figure 11 and compared with our model (Figure 9) for the Ru-

based oxygen reduction catalyst. The reaction centre of the hydrogenase, which reduces protons to hydrogen and catalyses a turnover of 10^6 protons per second at 30 °C, has only iron as metal centres and may nevertheless rival any noble metal hydrogen electrode. This is composed of an electron donating structure of three Fe_4S_4 and one Fe_2S_2 cluster which transfer electrons into the socalled H cluster composed of one Fe_4S_4 cluster and, surprisingly, to a Fe_2S_2 unit, in which each iron is sixfold coordinated, including two terminal CO or CN groups as in organometallic complexes. Alltogether, five CO (or CN) ligands are bound to the two-iron subcluster. If the five iron–sulfur centres are considered to have the function of an electron reservoir which are supplying electrons to a CO stabilized catalytic cluster, we are faced with a quite surprising analogy with our preliminary model for oxygen reduction via the Ru based catalyst. The iron sulfur cluster reservoir plays the role of the Ru colloids, the CO stabilized Fe_2S_2 cluster the role of the CO stabilized Ru-complexes which are involved in catalysis. Sulfur bridges (formed by cysteine) provide the electron transfer link between the reservoir and the CO-stabilized metal cluster, such as Se or S in our study.

If the metal atoms, Fe, as well as Ru, were not bonded to CO (or CN) they would be oxidized to iron oxide and ruthenium oxide respectively and loose their ability to remain catalytically active. As calculations with a model Ru complex have shown (Figure 10) interaction with CO (or CN) creates a complex in which electronic states are split by as much as 5 eV from the Fermi level. Electrons involved in this bonding are not affected further by electrochemical charge transfer. In other words, CO will not be oxidized like on a pure Ru surface within the potential range of 0.5–0.8 V vs NHE but will remain bonded. Simultaneously, catalytic electron transfer processes could proceed via the largely antibonding d-states of the Ru-complexes near the Fermi level. Here it is interesting to note that Ru can form stable carbonyl complexes and Pt cannot. This surprising difference in chemical behaviour can easily be explained with our model calculation (Figure 10) assuming a similar octahedral symmetry for a hypothetical Pt-carbonyl complex. In this case, due to the higher electron number in Pt, antibonding states above the energy gap would have been populated. This may destabilize the entire complex and may explain the absence of stable Pt-carbonyl complexes. This difference with respect to the formation of carbonyl complexes may basically be the origin of methanol insensitivity of highly structured Ru interphases or dispersed Ru catalyst particles. When carbonyl complexes can form they will be responsible for stability, selectivity and methanol insensitivity.

On the other hand, on an ideal, close packed Ru metal surface, as studied under high vacuum conditions, Ru-carbonyl coordination complexes may not be able to form. In contrast, atomically rough Ru metal surfaces as present in small particles, which can react with CO and related carbon species to restructure the electronic d-states, as shown in our model calculations (Figure 10), will be able to form the proposed surface states. This assumption also explains why the main carbonyl content of catalyst samples prepared by thermolysis of Ru carbonyl is not oxidized to CO_2 during oxygen reduction as to be expected from electrochemical CO stripping experiments [32] in which CO adsorbs to more ideal Ru interfaces. Pt cannot form such carbonyl compounds and may, thus, not be able to form carbonyl modified surface structures with higher d-state density which may favour interfacial coordination type of interactions and selectivity. A puzzle remaining concerns why sputtered Ru electrodes are also insensitive against methanol oxidation, as is evident from DEMS measurements in our laboratory. It may be that oxidation is initially possible at reactive sites which, however, immediately react with the CO intermediate to form the more stable Ru-carbonyl complex which is responsible for selective d-state mediated interfacial coordination chemistry.

Based on our comparison with a hydrogenase a key requirement for reduction catalysis would therefore be to properly bind the metal species with reactive ligands, which stabilize it, but are sufficiently small to allow parallel access of the species to be reduced. This has apparently been achieved in the hydrogenase reaction center by binding CO (or CN) to the iron and this is also suggested to happen at the carbonyl modified Ru interface of the catalysts, which we investigated. There is another interesting similarity between the hydrogenase and our model system (Figure 11). Electrons have to be efficiently transferred to the molecular catalytic

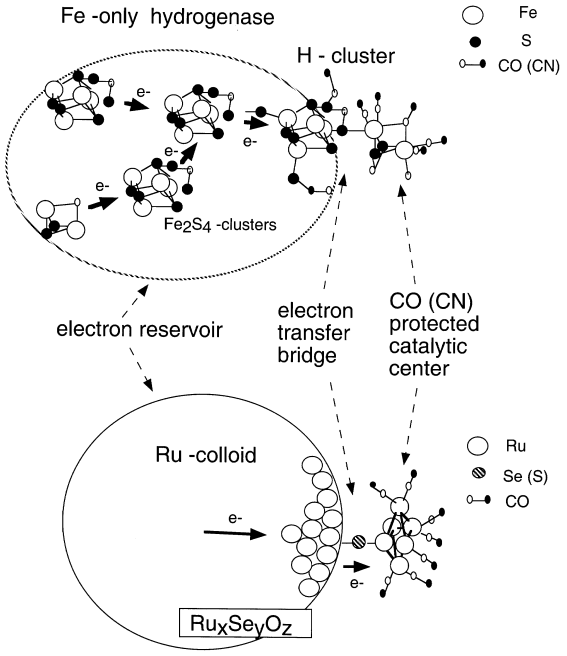

Fig. 11. Comparison of iron only hydrogenase (simplified) from a bacterium (Clostridium pasteurianum) compared with a proposed prototype of improved reduction catalysts. In both cases the cooperation of three entities, CO (or CN)-stabilized metal cluster, electron transfer bridge (–Se–, –S–, –S–S–) and of an electron reservoir (Ru metal colloid and Fe_4S_4 cluster aggregates) is evident.

centre. For this purpose molecular bridges for electron transfer are required. In biological catalysts sulfur bridges are used, based on cysteine. Selenium can be used in the investigated system, but it can be replaced by sulfur as shown with related catalysts, produced from metal carbonyls by thermolysis in xylene or similar solvents [14]. The third parallelism between the hydrogenase and the hypothetical Ru based oxygen reduction catalyst is the electron reservoir. Electrons must be readily available for the transfer to the catalytic centre. In the hydrogenase the array of iron–sulfur clusters supplies the electrons; in the Ru-based catalyst this role is played by the ruthenium metal colloids, which in our samples have a size of about 4 nm.

Both catalysts can also change their structure during electron exchange, which may give some autocatalytic, nonlinear component to electron transfer. There is much experimental opportunity to test this concept and to attempt further improvement of Ru based selective oxygen reduction catalysts [24]. Recent EXAFS measurements promise clarification of some of the questions posed [20].

Acknowledgement

This work was supported by the BMBF under contract 0327067B. We are indebted to K. Diesner for X-ray measurements and stimulating discussions, to A. Kurzweil for his assistance in mass spectrometric measurements and to U. Blöck for doing TEM investigations.

References

1. H. Collell, N. Alonso Vante and H. Tributsch, *J. Electroanal. Chem.* **324** (1992)127.
2. H. Tributsch, *Catalysis Today* **39** (1997) 177.
3. L. Pohlmann and H. Tributsch, *Electrochim. Acta*. **42** (1996) 2737.
4. H. Tributsch and L. Pohlmann, *Science* **279** (1998) 1891.
5. Alonso-Vante and H. Tributsch, *Nature* **323** (1986) 431.
6. R. Chevrel, Thèse, Serie B, No. 186/112 Universitè de Rennes (1974).
7. T. Hughbanks and R. Hoffmann, *J. Am. Chem. Soc.* **105** (1983) 115.
8. W. Seeliger, G.L. Throughton, N. Alonso-Vante and H. Tributsch, *J. Electrochem. Soc.* **142** (1995)166.
9. G. Faubert, G. Lalande, R. Coté, D. Guay, J.P. Dodelet, L.T. Weng, P. Bertrand and G. Dénès, *Electrochim. Acta* **41** (1996) 1689.
10. R.G. Egdell, J.B. Goodenough, A. Hamnett and C.C. Naish, *J. Chem. Soc. Faraday Trans.* **I 79** (1983) 89.
11. N. Alonso-Vante, M. Giersig and H. Tributsch, *J. Electrochem. Soc.* **138** (1991) 639.
12. N. Alonso-Vante, P. Bogdanoff and H. Tributsch, *J. Catalysis* (1999), submitted.
13. V. Trapp, P. Christensen and A. Hamnett, *J. Chem. Soc. Faraday Transac.* **92** (1996) 4311.
14. R.W. Reeve, P.A. Christensen, A.J. Dickinson, A. Hamnett and K. Scott, 3rd International Symposium on Electrocatalysis, Portoroz, Slovenia 12–15 Sept. 1999, to be published in *Electrochim. Acta.*
15. T.J. Schmidt, U.A. Paulus, H.A. Gasteiger and R.J. Behm, International Symposium on Electrocatalysis, Portoroz, Slovenia 12–15 Sept. 1999, to be published in *J. Appl. Electrochem.*
16. N. Alonso-Vante, Symposium on Electrocatalysis, Portoroz, Slovenia 12–15 Sept. 1999, to be published in *J. Appl. Electrochem.*
17. N. Alonso-Vante, M. Fieber Erdmann, H. Rossner, E. Holub-Krappe, C. Girogetti, A. Tadjedinne, E. Dartyge, A. Fontaine and R. Frahm, *J. Phys IV France* **7** (1997) C2-887.
18. H. Bönnemann , W. Brijoux, R. Brinkmann, E. Dinjus, T. Joussen and B. Korall. *Angew. Chem.* **103** (1991) N1.10 1344–46.
19. T.J. Schmidt, H.A. Gasteiger, G.D. Stäb, P.M. Urban, D.M. Kolb and R.J. Behm, *J. Electrochem. Soc.* **145** (1998) 2354.
20. S. Fiechter et al., to be published.
21. F. Piacenti, M. Bianchi and E. Benedetti, *Chem. Comm.* (1967) 775.
22. B.F.G. Johnson, R.D. Johnston and J. Lewis, *J. Chem. Soc.* A (1968) 2865.
23. B.F.G. Johnson, J. Lewis and I.G. Williams, *J. Chem. Soc.* A (1970) 901.
24. M. Bron, P. Bogdanoff, S. Fiechter, I. Dorbandt, M. Hilgendorff, H. Schulenburg and H. Tributsch, *J. Electroanal. Chem.* **500** (2001) 510.
25. E. Rupp, F. Nowak, S. Fiechter, G. Reck, V. Eyert, N. Alonso-Vante and H. Tributsch, *J. Chem. Soc. Dalton Trans.*, submitted.
26. P. Hänggi, P. Talkner and M. Borkovec, *Rev. Mod. Phys.* **62 (**251) (1990) 330.
27. S. Fiechter, P. Bogdanoff, M. Bron, I. Dorbandt, M. Hilgendorff, H. Schulenburg and H. Tributsch, to be published.
28. N.A. Anastasijevic, Z.M. Dinitrijevic and R.R. Adzić, *Electrochimica Acta* **31** (1986) 1125.
29. L.N. Nekrasov and E.I. Kruscheva, *Elektrokhimiya* **3** (1967) 166.
30. A.R. Williams, J. Kübler and C.D. Gelat, Jr. *Phys. Rev. B* **19** (1979) 6094.
31. J.W. Peters, W.N. Lanzilotta, B.J. Lemon and L.C. Seefeldt, *Science* **282** (1998) 1853.
32. W.F. Lin, T. Iwasita and W. Vielstich, *J. Phys. Chem. B* **103** (1999) 3250.